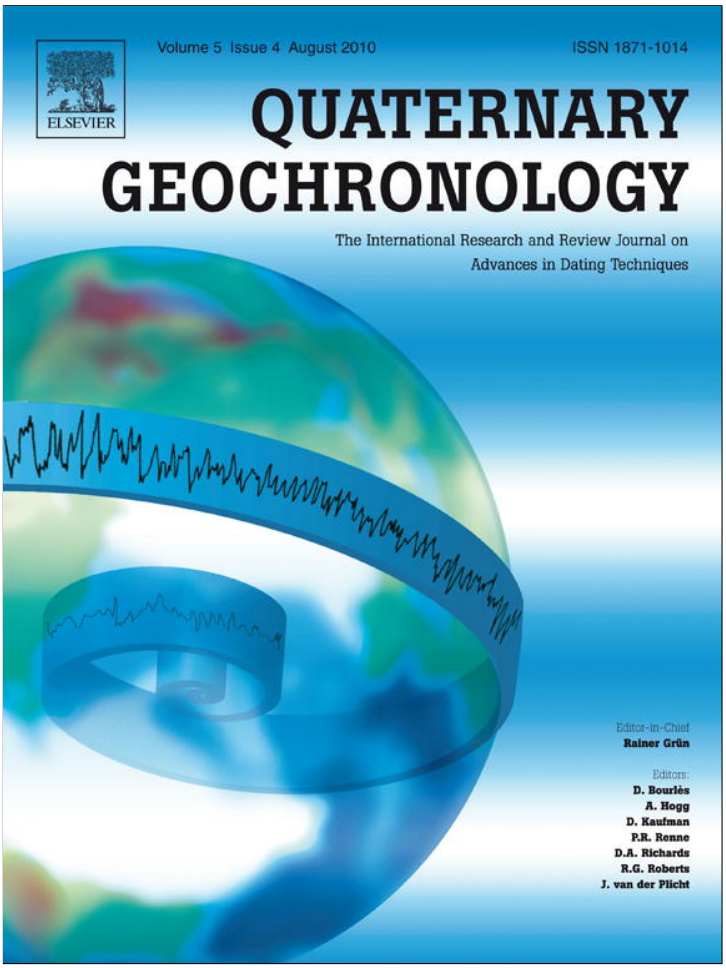

Quaternary Geochronology 5 (2010) 410–418

Contents lists available at ScienceDirect

Quaternary Geochronology

journal homepage: www.elsevier.com/locate/quageo

Research Paper

A reevaluation of *in situ* cosmogenic ^{3}He production rates

Brent M. Goehring [a,*], Mark D. Kurz [b], Greg Balco [c], Joerg M. Schaefer [a], Joseph Licciardi [d], Nathaniel Lifton [e]

[a] Department of Earth and Environmental Sciences and Lamont-Doherty Earth Observatory of Columbia University, 61 Route 9W, Palisades, NY 10964, USA
[b] Marine Chemistry and Geochemistry, Woods Hole Oceanographic Institution, Woods Hole, MA 02543, USA
[c] Berkeley Geochronology Center, 2455 Ridge Road, Berkeley, CA 94709, USA
[d] Department of Earth Sciences, University of New Hampshire, Durham, NH 03824, USA
[e] Department of Geosciences and Arizona AMS Facility, University of Arizona, Tucson, AZ 85721, USA

ARTICLE INFO

Article history:
Received 5 August 2009
Received in revised form
6 March 2010
Accepted 10 March 2010
Available online 15 March 2010

Keywords:
Helium-3
Cosmogenic nuclide
Exposure dating
Erosion rate

ABSTRACT

^{3}He is among the most commonly measured terrestrial cosmogenic nuclides, but an incomplete understanding of the ^{3}He production rate has limited robust interpretation of cosmogenic ^{3}He concentrations. We use new measurements of cosmogenic ^{3}He in olivine from a well-dated lava flow at Tabernacle Hill, Utah, USA, to calibrate the local ^{3}He production rate. The new ^{3}He measurements ($n = 8$) show excellent internal consistency and yield a sea level high latitude (SLHL) production rate of 123 ± 4 at g^{-1} yr^{-1} following the Lal (1991)/Stone (2000) scaling model [Lal, D., 1991. Cosmic ray labeling of erosion surfaces: *in situ* nuclide production rates and erosion models. Earth and Planetary Science Letters, 104, 424–439.; Stone, J.O., 2000. Air pressure and cosmogenic isotope production. Journal of Geophysical Research, 105, 23753–23759.]. We incorporate the new measurements from Tabernacle Hill in a compilation of all published production rate determinations, characterizing the mean global SLHL production rates (e.g. 120 ± 9.4 at g^{-1} yr^{-1} with Lal (1991)/Stone (2000)). The internal consistency of the global ^{3}He production rate dataset is as good as the other commonly used cosmogenic nuclides. Additionally, ^{3}He production rates in olivine and pyroxene agree within experimental error. The ^{3}He production rates are implemented in an age and erosion rate calculator, forming a new module of the CRONUS-Earth web-based calculator, a simple platform for cosmogenic nuclide data interpretation [Balco, G., Stone, J., Lifton, N.A., and Dunai, T.J., 2008. A complete and easily accessible means of calculating surface exposure ages or erosion rates from ^{10}Be and ^{26}Al measurements. Quaternary Geochronology, 3, 174–195.]. The ^{3}He calculator is available online at http://www.cronuscalculators.nmt.edu/.

1. Introduction

Helium-3 (^{3}He) was among the first terrestrial cosmogenic nuclides to be measured precisely (Craig and Poreda, 1986; Kurz, 1986a) and remains one of the most commonly measured cosmogenic nuclides for a variety of applications. Unlike other widely used cosmogenic nuclides (e.g. ^{10}Be, ^{26}Al, and ^{36}Cl), ^{3}He is stable, making it useful for surfaces of great antiquity. Moreover, the analytical detection limit of ^{3}He is low, allowing for precise measurements of very small amounts of cosmogenic ^{3}He. Cosmogenic ^{3}He and thus allows for the dating of surfaces ranging from hundreds to millions of years (e.g. Kurz and Geist, 1999; Schäfer et al., 1999, 2000; Licciardi et al., 2001, 2004, 2006). Because ^{3}He is quantitatively retained over geologic timescales in mafic minerals such as olivine and pyroxene (Trull et al., 1991; Brook and Kurz, 1993), the cosmogenic ^{3}He surface exposure dating technique is applicable to a variety of widespread surface lithologies, and is particularly useful where quartz-bearing lithologies are not available for ^{10}Be and ^{26}Al measurement.

Among the commonly measured terrestrial cosmogenic nuclides ^{3}He has the greatest number of production rate calibration measurements, distributed over wide latitudinal and altitudinal ranges (Fig. 1; Table 1), due to the availability of well-preserved basaltic lava flows with independent age control. Initial studies were carried out in the Hawaiian Islands (Kurz, 1986a; Kurz, 1986b, 1987; Kurz et al., 1990) and the western USA and France (Cerling, 1990; Poreda and Cerling, 1992; Cerling and Craig, 1994). Additional measurements have been made in Oregon, USA (Licciardi et al., 1999), the Canary Islands (Dunai and Wijbrans, 2000), Patagonia (Ackert et al., 2003), Iceland (Licciardi et al., 2006), and Hawaii and Mount Etna, Italy (Blard et al., 2006). Most of the previous studies have reported ^{3}He production rates based on the scaling schemes of Lal (1991) or Dunai (2001), but rarely for the other major scaling schemes (Lifton et al., 2005; Desilets et al.,

* Corresponding author. Tel.: +1 845 365 8572.
E-mail address: goehring@ldeo.columbia.edu (B.M. Goehring).

1871-1014/$ – see front matter © 2010 Elsevier B.V. All rights reserved.
doi:10.1016/j.quageo.2010.03.001

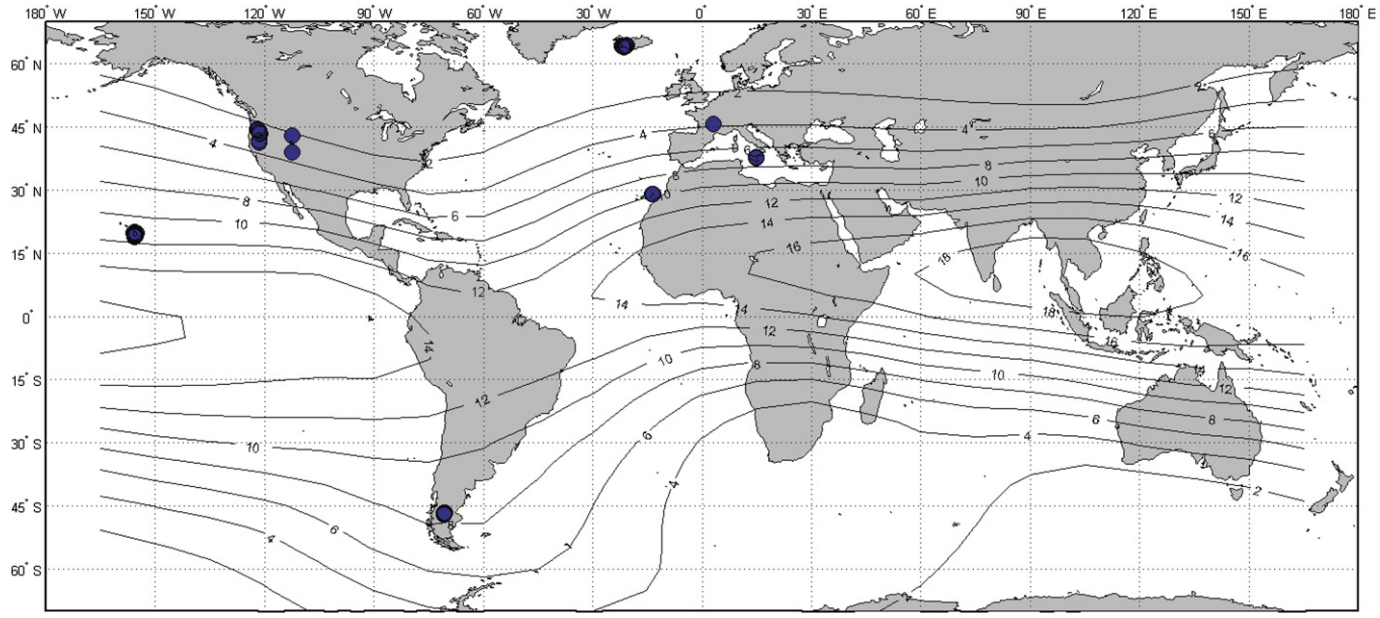

Fig. 1. Map showing locations of ^{3}He calibration samples. Most samples are located in the northern hemisphere mid-latitudes. Contours show the AD 1950 geomagnetic cutoff rigidity (GV; Lifton et al., 2005).

2006). For each of the commonly reported scaling schemes above, the studies show generally good agreement, but have never been incorporated into a single ^{3}He production rate estimate. In addition, the lack of a generally accepted means to interpret ^{3}He measurements as exposure ages or erosion rates in an internally consistent way has been a problem for cosmogenic ^{3}He studies.

^{3}He is produced via high-energy nuclear reactions in all mineral phases (Gayer et al., 2004, 2006; Amidon et al., 2007; Amidon et al., 2009), but olivine and pyroxene have been the most widely used due to their ^{3}He retentiveness over long timescales. Variation in the ^{3}He production rate between different target minerals remains unresolved (Lal, 1991; Masarik and Reedy, 1995; Masarik and Beer, 1999; Masarik, 2002; Kober et al., 2005). Compositional dependent production is not addressed here, since the existing and new ^{3}He production rate data from pyroxene and olivine do not span a large enough compositional range to establish statistical significance.

Here we describe a ^{3}He exposure age calculator and present new results from a production rate calibration site at Tabernacle Hill, Utah. We combine the new results from Tabernacle Hill with all previously published calibration data to determine global ^{3}He spallation production rates for the compiled calibration dataset. The new global ^{3}He production rates are then implemented in the CRONUS-Earth ^{3}He exposure age and erosion rate online calculator.

2. Exposure age and erosion rate calculator

As part of the CRONUS-Earth initiative, Balco et al. (2008) presented an easily accessible online platform for well-documented and consistent interpretation of ^{10}Be and ^{26}Al measurements. Their calculator is based on a global compilation of existing ^{10}Be and ^{26}Al production rate experiments and can be used to determine both exposure ages and erosion rates. The ^{3}He calculator developed here follows a similar conceptual approach and adapts the MATLAB code developed by Balco et al. (2008) for cosmogenic ^{3}He; input parameters are summarized in Table 2.

Exposure ages or erosion rates in the calculator are determined using five different scaling schemes. Production rates are also determined for the same five scaling schemes and for the remainder of this study we abbreviate as follows: 'Lal/Stone' = Stone (2000) following Lal (1991); 'Dunai' = Dunai (2001), 'Desilets' = Desilets et al. (2006), 'Lifton' = Lifton et al. (2005), and 'Lal-t' = the time-dependent adaptation of Lal (1991). The Lifton, Dunai, and Desilets scaling schemes are based on neutron monitor data and parameterized by estimates of effective vertical cutoff rigidity (R_C) and atmospheric depth. The Lal/Stone and Lal-t schemes are also based primarily on measurements from neutron monitors and other neutron detectors, but are normalized using

Table 1
Summary of previous studies used in calculation of production rates. All of these studies rely on independently dated surfaces. Cutoff rigidity (R_C) represents the AD 1950 value from Lifton et al. (2005). It is important to note that the SLHL production rates reported below were calculated using differing atmospheric models (e.g., the Iceland rate of 132 ± 5 is based on the standard atmosphere (*not* the NCEP-NCAR reanalysis with geographically variable mean sea-level pressure and 1000 mbar temperature fields) – the Iceland Lal/Stone value of 122 ± 6.1 reported in Table 5 is lower because of the use the NCEP-NCAR reanalysis product).

Study	Location	Latitude	Elevation range (m)	R_C (GV)	Reported SLHL production rate (at g^{-1} yr^{-1})	Scaling model
Kurz et al., 1990	Hawaii, USA	19.4	18–2339	11	125–127	Lal, 1991
Cerling, 1990; Poreda and Cerling, 1992; Cerling and Craig, 1994	Western USA and France	41.8	860–1455	3–4	115 ± 4	Lal, 1991
Licciardi et al., 1999	Oregon, USA	44.2	925–1622	3	116 ± 3	Lal, 1991
Dunai and Wijbrans, 2000	Canary Islands	28.9	30–197	10	118 ± 11	Dunai, 2000
Ackert et al., 2003	Argentina	−46.8	380–905	8	129–139	Lal, 1991/Stone, 2000
Licciardi et al., 2006	Iceland	64.1	22 to 459	<2	132 ± 5	Lal, 1991/Stone, 2000
Blard et al., 2006	Hawaii, USA and Mt Etna, Italy	19.4 and 37.7	40–3950	11 and 7	128 ± 5 136 ± 6	Lal, 1991/Stone, 2000 Dunai, 2001

Table 2
^{3}He exposure age and erosion rate calculator input parameters.

Input Parameter	Units
Sample ID	String
Latitude	Decimal Degrees
Longitude	Decimal Degrees
Elevation or pressure	m or hPa
Elevation/pressure flag[a]	String ('std', 'ant', or 'pre')
Sample thickness	cm
Sample density	g cm^{-3}
Shielding correction	Scalar between 0 and 1
Erosion rate[b]	cm yr^{-1}
^{3}He concentration	at g^{-1}
^{3}He concentration uncertainty	at g^{-1}

[a] Code identifies whether sample elevation is given, or if mean atmospheric pressure at the site is given. If an elevation is given, one must also select an atmospheric approximation for calculating atmospheric pressure. The 'std' code implements air pressure calculations using the ICAO standard atmosphere equation with sea level temperature and pressure derived from the NCEP-NCAR reanalysis product (http://www.cdc.noaa.gov/ncep_reanalysis/), 'ant' calculates air pressure for Antarctica using the model developed in Stone (2000) and is only appropriate for use with samples from Antarctica, 'pre' tells the calculator that site air pressure has been defined and should not be calculated. See Balco et al. (2008) for more details.
[b] An assumed erosion rate is not needed for erosion rate calculations.

nuclear disintegration data from photographic emulsions at different elevations and geomagnetic latitudes. The Desilets, Dunai, Lifton, and Lal-t scaling models incorporate temporal changes in the geomagnetic field, while the Lal/Stone model is not time dependent. For a complete discussion of the implementation of the scaling models and paleomagentic models, see Balco et al. (2008). We focus on the results of the Lal/Stone and Lifton scaling schemes in the text for brevity, and the fact that the Lal/Stone scheme has historically been the most widely used. Note that the Lifton scaling scheme exhibits very similar behavior to the other neutron monitor based models (Desilets and Dunai).

The ^{3}He production rates determined and discussed below assume production by spallation only, even though other production pathways are possible. We do not account for production of ^{3}He via muons due to the lack of either empirical muon production rate measurements or muogenic production cross-sections (e.g., as for ^{10}Be and ^{26}Al in Heisinger et al., 2002a,b). Lal (1987) reported theoretical estimates of ^{3}He production by muons to be ~2–3% of the total production at sea level high latitude (SLHL), therefore if production of ^{3}He by muons were later found to be significant, the values presented here would slightly overestimate spallogenic production. Data on the production of cosmogenic ^{3}He by muons, when they become available, can be implemented easily in the ^{3}He Online Calculator.

3. ^{3}He production rate measurements from Tabernacle Hill

3.1. Geological setting and ^{14}C chronology

Pluvial Lake Bonneville was a large lake that occupied the Bonneville Basin in Utah and easternmost Nevada during the late Pleistocene, of which the present-day Great Salt Lake and Utah Lake are remnants. The lake-level history is constrained by numerous radiocarbon dates on charcoal, macrofossils and tufa around the lake margin (e.g. Oviatt et al., 1992 and references therein; Godsey et al., 2005). The high stand of Lake Bonneville occurred between approximately 15.0–14.5 ^{14}C ka (Oviatt et al., 1992), and was terminated by the Bonneville Flood at ca. 14.5 ^{14}C ka. The Bonneville Flood resulted in a catastrophic drop in lake level of ~100 m, stabilizing at the level of the Provo shoreline complex until approximately 12.5 ^{14}C ka (Godsey et al., 2005).

The Tabernacle Hill basalt flow has previously been used as a primary ^{3}He production rate calibration site (Cerling, 1990; Poreda and Cerling, 1992; Cerling and Craig, 1994). The Tabernacle Hill flow is a small (~17 km^2), circular basalt exposure that was erupted into pluvial Lake Bonneville when the lake level was at or near the Provo shoreline level (Fig. 2), as indicated by the presence of glassy basalt pillows, tufa, and beach deposits around the flow margins (Oviatt and Nash, 1989; Godsey et al., 2005). Much of the Tabernacle Hill flow surface is well preserved and many primary flow surface features such as tumuli and pahoehoe ropes are present (Fig. 3). There is no evidence for submergence of the flow surface by Lake Bonneville; however, Sack (1999) and Godsey et al. (2005) presented stratigraphic evidence of an earlier transgressive still stand at or near the Provo level (ca. 20.8–17.7 ^{14}C ka). The exposure history of the Tabernacle Hill flow should be unaffected by such an interpretation, given that the eruption is inferred to have occurred at the Provo level and not during the earlier transgression.

The minimum age of the basalt flow is constrained by radiocarbon ages of 14.3 ± 0.1 ^{14}C ka (1σ) on dense tufa from the margin of the flow (Oviatt and Nash, 1989; Fig. 2). The flow cannot be older than the Bonneville Flood at 14.5 ± 0.1 ^{14}C ka when the lake rapidly drained from the Bonneville high stand to the Provo Shoreline level during the Bonneville Flood (Oviatt et al., 1992). Carbon reservoir effects were likely minimal (Broecker and Walton, 1959; Broecker and Kaufman, 1965) and therefore we include no correction; however, some have argued for increasing carbon reservoir ages as pluvial lake size decreased (Benson, 1993). We follow Lifton et al. (2001) and adopt the midpoint of the two ages above, 14.4 ± 0.2 ^{14}C ka, as the ^{14}C age of the flow, which corresponds to a calibrated 1σ age range of 17.0–17.6 cal ka (Reimer et al., 2004). We use the midpoint and range of the calibrated age to assign an age and best estimate of the uncertainty based on the age range of 17.3 ± 0.3 cal ka for the ^{3}He production rate calibration.

3.2. Methods

Samples were collected from the north side of the flow within 500 m of each other in order to obtain samples with uniform exposure history, although still far enough apart to identify potential site-specific issues such as shielding by soil or ash. All samples were derived from the tops of tumuli to minimize impacts of soil or tephra cover and to provide flat sampling surfaces to minimize surface slope corrections. A portable rock saw and hammer and chisel were used to collect the samples, which yielded consistent 4.5 cm thick samples. Topographic shielding measurements were made using a hand-held inclinometer – all were found to have zero topographic shielding correction and are therefore not reported.

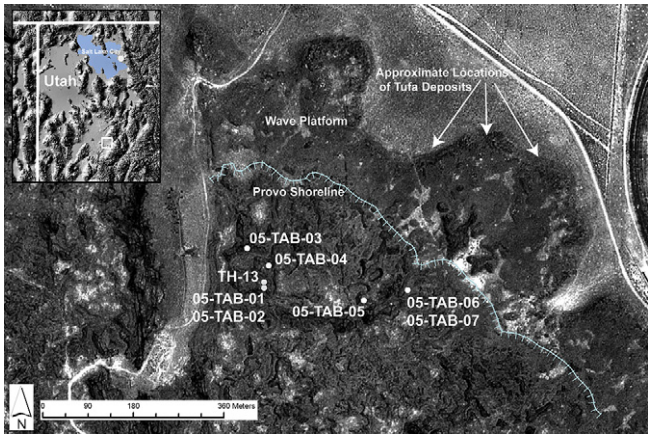

Fig. 2. Aerial photograph of northeastern portion of Tabernacle Hill flow showing locations of sampled surfaces. Also indicated is the approximate position of the Provo shoreline and wave platform, as well as locations of tufa deposits.

Fig. 3. Field photographs of Tabernacle Hill flow. A) Typical surface morphology of Tabernacle Hill flow showing minimal soil cover. B) Example of tufa material located along northern margin of flow. C) Example of a sampled surface. Well-preserved pahoehoe ropes visible. Sample surface is 05-TAB-06.

^{3}He concentrations in the Tabernacle Hill samples were measured at the Woods Hole Oceanographic Institution using a 90° magnetic sector noble gas mass spectrometer following previously published methods (Kurz, 1986b; Kurz et al., 1990; Kurz and Geist, 1999; Licciardi et al., 1999, 2006). To determine the quantity of cosmogenic ^{3}He and to separate non-cosmogenic (e.g. magmatic) helium components, phenocrysts were crushed in vacuo and the ^{3}He/^{4}He ratio determined. In a second step, the olivine powder was melted in a resistance furnace. The quantity of non-cosmogenic ^{3}He is calculated using the ^{3}He/^{4}He ratio measured during crushing and the total ^{4}He in the sample (Kurz, 1986a,b; Kurz et al., 1990):

$$^3\mathrm{He}_{\mathrm{inherited}} = \left(^3\mathrm{He}/^4\mathrm{He}\right)_{\mathrm{crushing}} \times {}^4\mathrm{He}_{\mathrm{total}}$$

The quantity of cosmogenic ^{3}He is then calculated using:

$$^3\mathrm{He}_{\mathrm{cosmogenic}} = {}^3\mathrm{He}_{\mathrm{total}} - {}^3\mathrm{He}_{\mathrm{inherited}}$$

3.3. Results

The new helium isotope data from six Tabernacle Hill samples show very consistent cosmogenic ^{3}He concentrations (Table 3), with an error-weighted mean of $(6.1 \pm 0.04) \times 10^6$ at g^{-1} (Fig. 4). This yields an error-weighted average local ^{3}He production rate of 352 ± 4 at g^{-1} yr^{-1} for ~1460 m altitude, ~38°N latitude, and ~120°W latitude. This new determination agrees well with the previously reported rate of 362 ± 6 at g^{-1} yr^{-1} (Cerling, 1990; Poreda and Cerling, 1992; Cerling and Craig, 1994). When scaled to SLHL assuming a standard atmosphere and sea level air pressure and 1000 mbar temperature from the NCAR/NCEP reanalysis data product (http://www.cdc.noaa.gov/ncep_reanalysis/), these are equivalent to reference ^{3}He production rates of 123 ± 4 at g^{-1} yr^{-1} for Lal (1991)/Stone (2000) and 136 ± 4 at g^{-1} yr^{-1} for Lifton et al. (2005; Table 4). Here and subsequently, by "reference ^{3}He production rate" we mean the ^{3}He production rate due to spallation at SLHL. Subsequent reference production rate determinations assume the standard atmosphere outlined above. All production rates presented in this study are reported with 1σ uncertainty, including 1σ analytical errors of the ^{3}He$_{cos}$ analysis, the ^{14}C analysis and resulting ^{14}C calibration uncertainty.

4. Global ^{3}He production rate calibration dataset

We next considered the new Tabernacle Hill data with published ^{3}He production rate datasets compiled from previous studies (Cerling, 1990; Kurz et al., 1990; Poreda and Cerling, 1992; Cerling and Craig, 1994; Licciardi et al., 1999, 2006; Dunai and Wijbrans, 2000; Ackert et al., 2003; Blard et al., 2006). Amidon et al. (2009) recently presented measurements of ^{3}He production olivine and pyroxene and ^{10}Be from quartz separated from the same exposed rocks, yielding a ^{3}He/^{10}Be production ratio. Based on the assumption that the ^{10}Be production rate is well known, they derived ^{3}He production rates. We choose not to include their data in this compilation as recent studies (Balco et al., 2009; Putnam et al., 2010) of the ^{10}Be production rate may indicate that the ^{10}Be production rate is less well-constrained than previously believed (see below). All but one of the published calibration samples come from independently dated basalt flows and include ^{3}He data from both olivine phenocrysts, while some also include measurements of ^{3}He from pyroxene phenocrysts. Independent age control of the lava flows comes from ^{40}Ar/^{39}Ar or K–Ar ages of the sampled flows or radiocarbon dating of material associated with flow emplacement. Published ^{14}C ages reported in the original publications have been recalibrated here to calendar ages using the CALIB 5.0.2

Table 3
Sample information for new Tabernacle Hill measurements. All uncertainties reported at 1σ. Duplicate measurements of 05-TAB-05 and 05-TAB-07 were averaged. All samples are 0.5–1.0 mm olivine phenocrysts. 05-TAB-05-grains were uncrushed before melting. 05-TAB-07-GM were selected to have adhering groundmass in order to test the influence of radiogenic ^{4}He from U and Th in the groundmass via α-implantation. This measurement yielded identical results to the other duplicate, which had only trace amounts of groundmass, demonstrating that radiogenic helium appears to be a negligible influence for this sample.

Sample	Latitude (°N)	Longitude (°W)	Elevation (m)	Thickness (cm)	Density (g cm^{-3})	Weight crush (g)	^{4}He (10^{-9} ccSTP g^{-1})	^{3}He/^{4}He ($R/R_{a,crush}$)	Weight melt (g)	^{4}He (10^{-9} ccSTP g^{-1})	^{3}He/^{4}He ($R/R_{a,melt}$)	^{3}He$_c$ (10^6 at g^{-1})
TH-13	38.9302	112.5222	1461	2.0	2.0	0.27025	8.34	6.10 ± 0.08	0.26225	8.46 ± 0.09	26.06 ± 0.19	6.28 ± 0.11
05-TAB-02	38.9301	112.5222	1463	4.5	2.04	0.24143	12.41	5.78 ± 0.06	0.22908	3.03 ± 0.05	57.94 ± 0.37	5.89 ± 0.12
05-TAB-04	38.9305	112.5221	1457	4.5	1.92	0.27506	10.55	5.86 ± 0.05	0.26222	3.38 ± 0.05	54.32 ± 0.35	6.10 ± 0.11
05-TAB-01	38.9301	112.5222	1463	4.5	2.8	0.26603	12.76	5.82 ± 0.09	0.25582	5.02 ± 0.06	38.33 ± 0.28	6.07 ± 0.10
05-TAB-05	38.9299	112.5199	1455	4.5	2.0	0.26075	14.80	5.60 ± 0.08	0.2504	4.27 ± 0.06	44.85 ± 0.38	6.18 ± 0.12
05-TAB-grains	"	"	"	"	"	–	–	–	0.16693	12.21 ± 0.14	19.62 ± 0.16	6.20 ± 0.12
											Average	**6.19±0.08**
05-TAB-06	38.9301	112.5189	1457	4.5	2.18	0.26404	11.10	6.03 ± 0.06	0.25536	2.31 ± 0.05	78.82 ± 0.91	6.27 ± 0.15
05-TAB-03	38.9308	112.5226	1461	4.5	2.11	0.28442	9.96	5.75 ± 0.08	0.27861	9.19 ± 0.10	23.30 ± 0.14	6.00 ± 0.10
05-TAB-07	38.9301	112.5189	1457	4.5	2.03	0.25313	14.40	5.89 ± 0.06	0.2443	3.57 ± 0.05	51.21 ± 0.33	6.02 ± 0.11
05-TAB-07-GM	"	"	"	"	"	0.22199	34.09	6.16 ± 0.05	0.2151	7.84 ± 0.09	26.36 ± 0.16	5.89 ± 0.10
											Average	**5.96±0.09**

radiocarbon calibration program (Reimer et al., 2004). From the total of 37 sampled flows/surfaces, we initially only exclude two: the altitudinal transect of the ~1500 yr old flow of Blard et al. (2006) due to the uncertain age control and small quantities of cosmogenic ^{3}He, and the 1.35 Ma flow investigated by Dunai and Wijbrans (2000) due to large uncertainties regarding surface erosion of this old flow. We include here only selected samples from the original Hawaii dataset by Kurz et al. (1990), judged using the quality rating in Kurz et al. (1990) to have good surface preservation (only retained samples with quality rating 1). Some of the studies do not report all required information for use in the calculator. In these cases, we use the reported ^{3}He concentrations and assume they have been corrected for sample thickness and calculated for zero erosion and no shielding. No corrections have been made for isostatic rebound or subsidence. Samples with multiple measurements were averaged (error-weighted) and treated as a single sample. Table 1 summarizes the locations, site description(s), scaling model originally used in calibration, and resulting site-specific production rates. The full dataset is presented in the Supplementary Online Material.

4.1. Data fitting

To determine summary reference ^{3}He production-rate values for the combined new Tabernacle Hill and previously published datasets, we grouped sites by geographic region, instead of by individual studies. For example, the western North America region includes the new Tabernacle Hill measurements reported here and previously reported for Tabernacle Hill (Cerling, 1990; Poreda and Cerling, 1992; Cerling and Craig, 1994) from Belknap Crater and Gilmore, OR, Medicine Lake, CA, Bonneville Flood deposits in Pocatello, Idaho, and Tabernacle Hill, Utah, and Licciardi et al. (1999) data from Oregon. To determine the best-fitting reference production rates to the data in each region, we used the least-squares minimization method described by Balco et al. (2009), which identifies the ^{3}He production rate that minimizes the misfit between the calculated and independently determined exposure ages for calibration samples at a given site. We argue that this approach, which is similar to taking the error-weighted mean is justified because the results from a particular region are replicate measurements of the same thing (since scaling uncertainties are minimized). To determine a summary reference production rate and uncertainty for the entire dataset, we then computed the arithmetic mean and standard deviation of the reference production rates determined from the individual regions. We take this averaging approach because the scatter of the region means is the only means of estimating the scaling uncertainty. The scaling uncertainty we obtain is larger than most of the regional dataset uncertainties, so the summary production rate value should use the scaling uncertainty inferred from the scatter of the regional dataset means. Additionally, the means of the regional datasets do not form a single population and therefore we cannot take the weighted mean of the regional dataset values as the summary value.

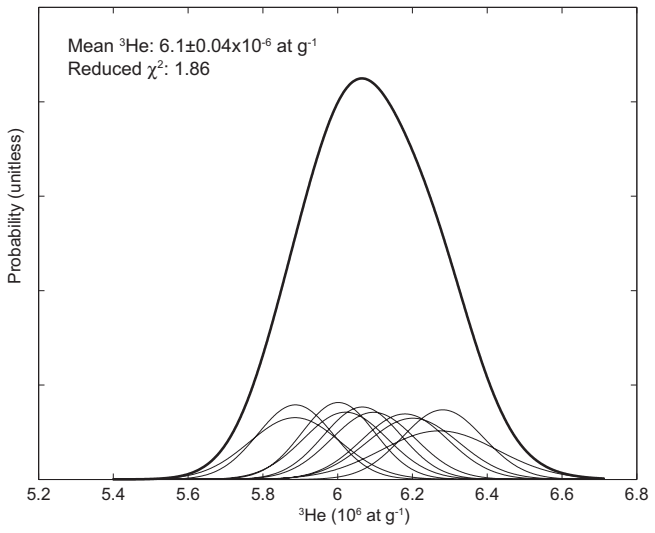

Fig. 4. Individual and summary probability density function (PDF) for new ^{3}He production rate measurements from Tabernacle Hill, Utah.

5. Results and discussion

Calculated best-fit reference ^{3}He production rates for the regional datasets are summarized in Table 5 and Fig. 5. We also report in the Supplementary Online data reference ^{3}He production rates for each of the previously published studies used in the compiled dataset for interest and comparison with previously

Table 4
Reference best-fitting SLHL ^{3}He production rates for the new Tabernacle Hill samples.

Scaling model	^{3}He prod. rate (at g^{-1} yr^{-1})	χ^2_ν
Lal/Stone	123 ± 3.5	0.55
Desilets	126 ± 3.7	0.50
Dunai	125 ± 3.7	0.49
Lifton	136 ± 4.1	0.49
Lal-t	119 ± 3.5	0.51

Table 5
Best-fitting reference ^{3}He production rates from each of the regions for olivine, pyroxene, and the ^{3}He concentrations from two mineral phases combined. All uncertainties reported at 1σ. Scaling models have been abbreviated here and in Table 6 as follows: Lal/Stone, Desilets, Dunai, Lifton, and Lal-t.

Scaling model	Ol ^{3}He prod. rate (at g^{-1} yr^{-1})	χ^2_υ	Px ^{3}He prod. rate (at g^{-1} yr^{-1})	χ^2_υ	Ol + Px ^{3}He prod. rate (at g^{-1} yr^{-1})	χ^2_υ
Western North America (Tabernacle Hill this study, Cerling and Craig, 1994[a]; Licciardi et al., 1999; Poreda and Cerling, 1992)						
Lal/Stone	115 ± 4.4	5.4	92 ± 4.6	1.8	–	–
Desilets	120 ± 4.8	4.0	96 ± 5.0	1.9	–	–
Dunai	121 ± 4.8	4.2	97 ± 5.1	1.9	–	–
Lifton	130 ± 5.2	4.3	103 ± 5.3	2.0	–	–
Lal-t	114 ± 4.5	3.7	89 ± 4.1	2.8	–	–
Southern South America (Ackert et al., 2003[a])						
Lal/Stone	129 ± 4.6	1.9	130 ± 3.6	0.33	130 ± 4.4	1.4
Desilets	131 ± 4.7	2.1	132 ± 3.8	0.34	132 ± 4.6	1.5
Dunai	133 ± 4.7	2.1	134 ± 3.8	0.34	133 ± 4.6	1.5
Lifton	140 ± 5.1	2.1	141 ± 4.1	0.35	140 ± 4.9	1.5
Lal-t	125 ± 4.5	1.9	126 ± 3.6	0.34	125 ± 4.3	1.3
Canary Islands (Dunai and Wijbrans, 2000)						
Lal/Stone	103 ± 11.9	0.06	–	–	–	–
Desilets	106 ± 12.3	0.06	–	–	–	–
Dunai	101 ± 11.8	0.06	–	–	–	–
Lifton	112 ± 13.0	0.07	–	–	–	–
Lal-t	92 ± 10.7	0.07	–	–	–	–
Iceland (Licciardi et al., 2006)						
Lal/Stone	122 ± 6.1	2.3	–	–	–	–
Desilets	126 ± 6.3	2.3	–	–	–	–
Dunai	125 ± 6.3	2.3	–	–	–	–
Lifton	134 ± 6.7	2.3	–	–	–	–
Lal-t	122 ± 6.1	2.3	–	–	–	–
Hawaii (Kurz et al., 1990; Blard et al., 2006)						
Lal/Stone	124 ± 13	12	–	–	–	–
Desilets	140 ± 15	11	–	–	–	–
Dunai	135 ± 14	11	–	–	–	–
Lifton	155 ± 17	11	–	–	–	–
Lal-t	126 ± 13	9	–	–	–	–
Europe (Cerling and Craig, 1994[a]; Blard et al., 2006[a])						
Lal/Stone	135 ± 7.6	4.4	117 ± 6.9	11	123 ± 8.3	7.9
Desilets	139 ± 8.1	4.0	123 ± 7.2	10	129 ± 8.6	6.9
Dunai	139 ± 8.1	4.0	123 ± 7.1	8.8	128 ± 8.3	6.1
Lifton	151 ± 8.8	4.0	133 ± 7.8	10	139 ± 9.3	6.9
Lal-t	128 ± 7.3	4.1	112 ± 6.6	9.7	118 ± 7.9	6.7

[a] Study reports separate ^{3}He measurements in olivine and pyroxene.

published values. All of the regional datasets are within 1σ of the grand mean and 1 standard deviation of all of the data (Fig. 5). We therefore include all of the regional datasets in the production rate estimates below.

Based on our combined dataset, we derive reference SLHL production rates of 121 ± 11 at g^{-1} yr^{-1} and 137 ± 16 at g^{-1} yr^{-1} for Lal/Stone and Lifton respectively for olivine and 113 ± 18 at g^{-1} yr^{-1} for St and 125 ± 19 at g^{-1} yr^{-1} for Li in pyroxene (Table 6). Production rates from pyroxene alone exhibit much greater scatter than the olivine-only dataset. The pyroxene ^{3}He production rates from South America and Europe are in close agreement, while the pyroxene ^{3}He production rate from western North America is significantly lower (~25%; Table 5). The pyroxenes from all three regions are clinopyroxene, primarily augite, and thus production rate variations due to compositional differences should be minimal (Ackert et al., 2003; Bacon and Lanphere, 2006; Blard et al., 2006). The lower ^{3}He production rate for the North America samples (Mount Mazama ash) could be explained by higher erosion of the ash relative to that of the lava flows from which the other pyroxene samples come from; the pyroxene production rate estimate from the Mount Mazama ash may therefore be an underestimate and we do not discuss further. In sum, this yields a ^{3}He production rate in the remaining samples of pyroxene of 124 ± 9.2 at g^{-1} yr^{-1} for Lal/Stone and 137 ± 5.7 at g^{-1} yr^{-1} for Lifton, indistinguishable from the olivine ^{3}He production rates of 121 ± 11 at g^{-1} yr^{-1} and 137 ± 16 at g^{-1} yr^{-1} for Lal/Stone and Lifton, respectively.

The observed general agreement between olivine and pyroxene ^{3}He production rates is consistent with theoretical estimates (e.g. Masarik and Reedy, 1995; Masarik and Beer, 1999; Masarik, 2002), which predict only slightly different SLHL production rates for olivine and pyroxene (115 at g^{-1} yr^{-1} vs. 119 at g^{-1} yr^{-1}). However, our results deviate from the estimated SLHL production rates of ~161 at g^{-1} yr^{-1} and ~136 at g^{-1} yr^{-1} for olivine and pyroxene, respectively, predicted by the model of Kober et al. (2005). Recent measurements of ^{3}He production in olivine and pyroxene calibrated against ^{10}Be production in quartz from the same rock (Amidon et al., 2009) indicate essentially no difference in ^{3}He production rates between the two mineral phases, supporting our results. However, Amidon et al. (2009) report higher absolute ^{3}He production rates for Lal/Stone of 145 ± 11 at g^{-1} yr^{-1} and 141 ± 16 at g^{-1} yr^{-1} than our estimates for olivine and pyroxene, respectively, based on the measured ^{3}He/^{10}Be production rate ratio and on the ^{10}Be production rates reported in Balco et al. (2008). Use of the lower ^{10}Be production rates reported in two recent studies (Balco et al., 2009; Putnam et al., 2010) would lower the Amidon et al. (2009) ^{3}He production rates to 125 ± 10 and 122 ± 14 at g^{-1} yr^{-1} for olivine and pyroxene respectively, in agreement with our results above.

Given these results above, we combined the olivine and pyroxene datasets. The resulting calculated SLHL ^{3}He production rate for the Lal/Stone scaling scheme is 120 ± 9.4 at g^{-1} yr^{-1} (7.8%) and 135 ± 14 at g^{-1} yr^{-1} (10.4%) for the Lifton scaling scheme (Fig. 6). The 8–11% uncertainty associated with our conservative

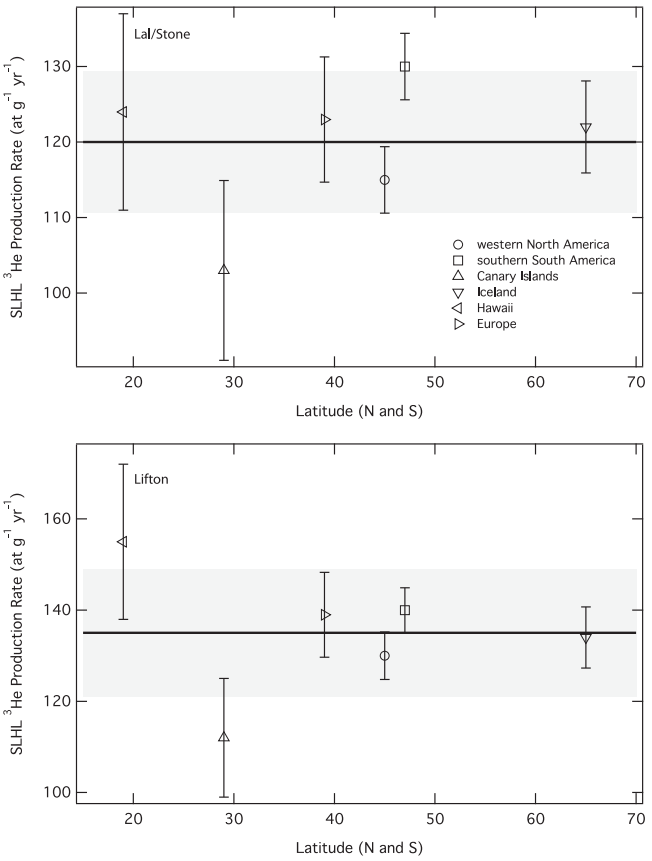

Fig. 5. Regional production rates for the Lal/Stone and Lifton scaling schemes, including the new Tabernacle Hill data. Only the Lal/Stone and Lifton schemes are shown for brevity – the Desilets and Dunai scaling schemes yield similar results. Best-fit global production rate and 1σ uncertainty indicated by the solid horizontal line and shaded areas.

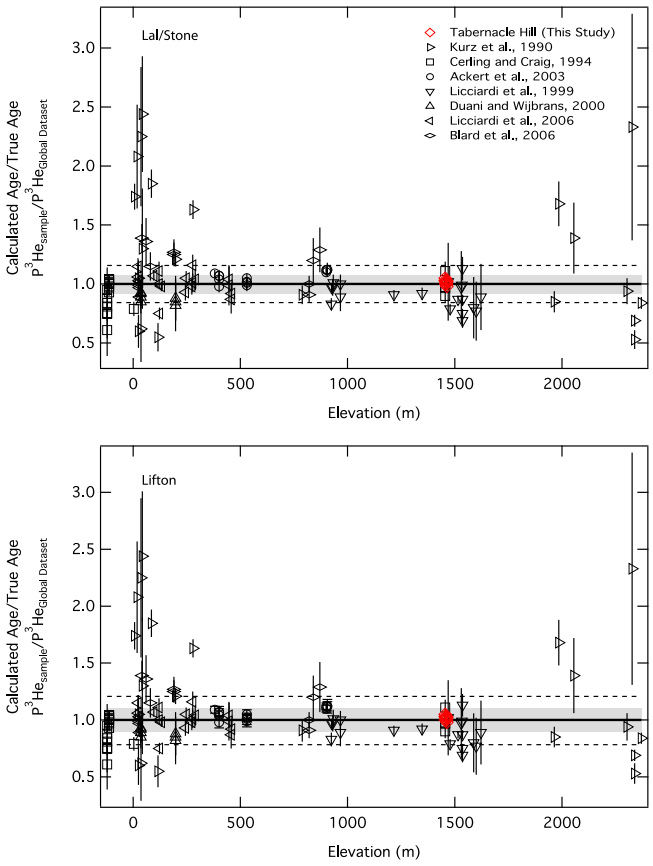

Fig. 6. Fit of representative scaling schemes to the new Tabernacle Hill and global calibration dataset. Only the Lal/Stone and Lifton schemes are shown for brevity – the Desilets and Dunai scaling schemes yield similar results. Each data point shows the ratio of the exposure age calculated from the ^{3}He concentration at a calibration site, using the best-fit production rates determined from the global dataset in Table 5, to the independently determined exposure age of the site. Because of the stable nature of ^{3}He, this is equivalent to the ratio of the production rate inferred from a particular site and the production rate that best-fits the entire dataset. Therefore, samples with ratios greater than one have production rates greater than the average for the entire dataset. The error bars represent 1σ uncertainties. The gray band reflects the 1σ uncertainty in the best-fit production rate from Table 6.

treatment of the ^{3}He production rate dataset is comparable to that exhibited by the ^{10}Be dataset in Balco et al. (2008). However, it is important to recognize that much of the scatter is the result of the Hawaii and Canary Island sample regions. The difference between these two regions and those in the mid- to high-latitudes could be a result of scaling inadequacies; however, it could also be the result of poorer geomorphic preservation and/or poorer age control. The quality of production rate calibrations for both ^{3}He and ^{10}Be should be improving in the near future as new calibration sites are identified (e.g. Balco et al., 2009) and the CRONUS-Earth efforts become available.

Table 6
Summary reference ^{3}He production rates calculated from arithmetic mean and standard deviations of the reference regional production rates.

Scaling model	^{3}He production rate (at g^{-1} yr^{-1})	χ^2_ν
Olivine and Pyroxene		
Lal/Stone	120 ± 9.4	1.8
Desilets	126 ± 12	1.4
Dunai	124 ± 12	1.8
Lifton	135 ± 14	1.3
Lal-t	116 ± 13	2.2
Olivine		
Lal/Stone	121 ± 11	2.1
Desilets	127 ± 13	1.7
Dunai	126 ± 14	2.2
Lifton	137 ± 16	1.9
Lal-t	118 ± 14	2.4
Pyroxene		
Lal/Stone	124 ± 9.2	4.1
Desilets	128 ± 6.4	1.8
Dunai	129 ± 7.8	2.7
Lifton	137 ± 5.7	1.2
Lal-t	119 ± 9.9	4.9

We implement in the online exposure age and erosion rate calculator reference summary ^{3}He production rates presented in Table 5. The calculator is available at http://www.cronuscalculators.nmt.edu/, and can be used to calculate exposure ages and steady state erosion rates in a simple and internally consistent manner. This will enable internally consistent comparisons of exposure ages and erosion rates based on ^{3}He and other cosmogenic nuclides (e.g. ^{10}Be and ^{26}Al) determined with the companion calculator. For each scaling scheme an internal and external uncertainty are reported. The former includes analytical uncertainty only, while the latter includes analytical and production rate uncertainty.

Blard et al. (2006) presented results suggesting that cosmogenic ^{3}He may be lost during initial in vacuo cold crushing, thereby possibly lowering the measured cosmogenic ^{3}He concentration and leading to an underestimate of the ^{3}He production rate. Both the Hawaii and Europe datasets include measurements from Blard et al. (2006) and are in agreement at 1σ with the rest of the ^{3}He dataset

(Fig. 5), suggesting that cosmogenic ^{3}He loss during crushing is not a major problem. In addition, sample 05-TAB-05 has been measured with both cold crushing prior to fusion and fusion of whole grains (without prior crushing), with no significant difference in cosmogenic ^{3}He contents, supporting previous reports that loss during crushing is insignificant (Fig. 4; Kurz, 1986b; Licciardi et al., 1999, 2006).

Blard and Farley (2008) assessed the potential impact of radiogenic ^{4}He on all but one of the previously published studies and found that radiogenic ^{4}He production following helium closure is minimal (1–5% underestimation) due to the low U and Th contents of the flows used in this study and therefore no corrections have been made for radiogenic ^{4}He. The low U and Th contents of most rocks containing olivine also make production via thermal neutron capture on ^{6}Li relatively minor (Amidon et al., 2007; Dunai et al., 2007), and thus have not been accounted for in our production rate estimates. Additionally, the low Li contents typical of the basaltic lava flows in this compilation also minimize cosmogenic production of ^{3}He by thermal neutron capture on ^{6}Li.

6. Potential complications

Surfaces with similar ages and lithologies to those used in the calibration of the ^{3}He production produce reliable exposure ages with few complications. However, as the age of the rock increases and/or its lithology becomes more complex, ^{3}He exposure dating becomes more complicated. One potential complication is that as the age of the rock gets older (not necessarily exposure age) and the U and Th contents becomes higher, the radiogenic ^{4}He correction as proposed by Blard and Farley (2008) becomes more important. The online calculator does not currently make these corrections. A second potential complication is that unlike most of the flows used in the production rate estimates above, lavas derived from crustal sources can contain significantly more U, Th, and Li and therefore ^{3}He produced from reactions with Li can comprise a significant portion of the measured ^{3}He signal. Because of the potential of ^{3}He production via reaction with Li, the calculator is likely not applicable to rocks with very old (>5 Myr) helium closure ages, and/or for rocks that are enriched in Li, unless a shielded sample is used and Li, U, and Th is measured to correct the ^{3}He concentration for these production mechanisms.

7. Conclusions

New measurements of the SLHL ^{3}He production rates from the well-dated Tabernacle Hill (Utah, USA) lava flow show high internal consistency and are in excellent agreement with previously published rates from the same location (Cerling, 1990; Poreda and Cerling, 1992; Cerling and Craig, 1994). The new measurements are combined with published data, and we present a global compilation of *in situ* ^{3}He production rate estimates. Additionally, there is no demonstrable difference in ^{3}He production rates in olivine and pyroxene. The global production rates are implemented in a ^{3}He exposure age and erosion rate calculator as a new module of the CRONUS-Earth web calculator (Balco et al., 2008). Although these results are encouraging, more ^{3}He production rate calibration sites are needed that have excellent age control, pristine surface preservation, and span a wider range of elevations and latitudes.

Acknowledgements

We thank Pierre-Henri Blard and William Amidon for constructive reviews that improved this manuscript. BMG was funded by a CRONUS-Earth Graduate Research Fellowship. JMS, MK, and NL acknowledge support by the NSF (EAR # 0345595, 0345835, and 0345150). This is LDEO publication #7323.

Appendix. Supplementary data

Supplementary data associated with this article can be found in the online version, at doi:10.1016/j.quageo.2010.03.001.

Editorial handling by: D. Bourlès

References

Ackert, R.P., Singer, B., Guillou, H., Kaplan, M., Kurz, M., 2003. Long-term cosmogenic ^{3}He production rates from ^{40}Ar/^{39}Ar and K–Ar dated Patagonian lava flows at 47°S. Earth and Planetary Science Letters 210, 119–136.

Amidon, W., Farley, K., Burbank, D., Pratt-Sitaula, B., 2007. Anomalous cosmogenic 3He production and elevation scaling in the high Himalaya. Earth and Planetary Science Letters 265, 287–301.

Amidon, W.H., Rood, D.H., Farley, K.A., 2009. Cosmogenic 3He and 21Ne production rates calibrated against 10Be in minerals from the Coso volcanic field. Earth and Planetary Science Letters 280, 194–204.

Bacon, C.R., Lanphere, M.A., 2006. Eruptive history and geochronology of Mount Mazama and the Crater Lake region, Oregon. Geological Society of America Bulletin 118, 1331–1359.

Balco, G., Stone, J., Lifton, N.A., Dunai, T.J., 2008. A complete and easily accessible means of calculating surface exposure ages or erosion rates from ^{10}Be and ^{26}Al measurements. Quaternary Geochronology 3, 174–195.

Balco, G., Briner, J., Finkel, R.C., Rayburn, J.A., Ridge, J.C., Schaefer, J.M., 2009. Regional beryllium-10 production rate calibration for late-glacial Northeastern North America. Quaternary Geochronology 4, 93–107.

Benson, L., 1993. Factors affecting 14C ages of lacustrine carbonates: timing and duration of the last highstand lake in the Lahontan Basin. Quaternary Research 39, 163–174.

Blard, P.H., Farley, K.A., 2008. The influence of radiogenic ^{4}He on cosmogenic ^{3}He determinations in volcanic olivine and pyroxene. Earth and Planetary Science Letters 276, 20–29.

Blard, P., Pik, R., Lave, J., Bourles, D., Burnard, P., Yokochi, R., Marty, B., Trusdell, F., 2006. Cosmogenic ^{3}He production rates revisited from evidences of grain size dependent release of matrix-sited helium. Earth and Planetary Science Letters 247, 222–234.

Broecker, W.S., Kaufman, A., 1965. radiocarbon chronology of Lake Lahontan and Lake Bonneville II, Great Basin. Geological Society of America Bulletin 76, 537.

Broecker, W.S., Walton, A., 1959. The geochemistry of C14 in fresh-water systems. Geochimica et Cosmochimica Acta 16, 15–38.

Brook, E.J., Kurz, M.D., 1993. Surface-Exposure Chronology using in situ cosmogenic 3He in Antarctic quartz Sandstone Boulders. Quaternary Research 39, 1–10.

Cerling, T.E., Craig, H., 1994. Cosmogenic ^{3}He production rates from 39°N to 46°N latitude, western USA and France. Geochimica et Cosmochimica Acta 58, 249–255.

Cerling, T.E., 1990. Dating Geomorphologic surfaces using cosmogenic He-3 dating. Quaternary Research 33, 148–156.

Craig, H., Poreda, R.J., 1986. Cosmogenic He-3 in terrestrial rocks-the summit lavas of Maui. Procedings of the National Acadamey of Science 83, 1970–1974.

Desilets, D., Zreda, M., Prabu, T., 2006. Extended scaling factors for in situ cosmogenic nuclides: new measurements at low latitude. Earth and Planetary Science Letters 246, 265–276.

Dunai, T.J., Wijbrans, J.R., 2000. Long-term cosmogenic ^{3}He production rates (152 ka–1.35 Ma) from ^{40}Ar/^{39}Ar dated basalt flows at 29°N latitude. Earth and Planetary Science Letters 176, 147–156.

Dunai, T.J., Stuart, F.M., Pik, R., Burnard, P., Gayer, E., 2007. Production of He-3 in crustal rocks by cosmogenic thermal neutrons. Earth and Planetary Science Letters 258, 228–236.

Dunai, T.J., 2001. Scaling factors for production rates of in situ produced cosmogenic nuclides: a critical reevaluation. Earth and Planetary Science Letters 176, 157–169.

Gayer, E., Pik, R., Lavé, J., France-Lanord, C., Bourles, D., Marty, B., 2004. Cosmogenic 3He in Himalayan garnets indicating an altitude dependence of the 3He/10Be production ratio. Earth and Planetary Science Letters 229, 91–104.

Gayer, E., Lavé, J., Pik, R., France-Lanord, C., 2006. Monsoonal forcing of Holocene glacier fluctuations in Ganesh Himal (Central Nepal) constrained by cosmogenic 3He exposure ages of garnets. Earth and Planetary Science Letters 252, 275–288.

Godsey, H.S., Currey, D.R., Chan, M.A., 2005. New evidence for an extended occupation of the Provo shoreline and implications for regional climate change, Pleistocene Lake Bonneville, Utah, USA. Quaternary Research 63, 212–223.

Heisinger, B., Lal, D., Jull, A.J.T., Kubik, P., Ivy-Ochs, S., Knie, K., Nolte, E., 2002a. Production of selected cosmogenic radionuclides by muons: 2. Capture of negative muons. Earth and Planetary Science Letters 200, 357–369.

Heisinger, B., Lal, D., Jull, A.J.T., Kubik, P., Ivy-Ochs, S., Neumaier, S., Knie, K., Lazarev, V., Nolte, E., 2002b. Production of selected cosmogenic radionuclides by muons: 1. Fast muons. Earth and Planetary Science Letters 200, 345–355.

Kober, F., Ivy-Ochs, S., Leya, I., Baur, H., Magna, T., Wieler, R., Kubik, P.W., 2005. In situ cosmogenic ^{10}Be and ^{21}Ne in sanidine and in situ cosmogenic ^{3}He in Fe-Ti-oxide minerals. Earth and Planetary Science Letters 236, 404–418.

Kurz, M.D., Geist, D., 1999. Dynamics of the Galapagos hotspot from helium isotope geochemistry. Geochimica et Cosmochimica Acta.

Kurz, M., Colodner, D., Trull, T.W., Moore, R.B., O'Brien, K., 1990. Cosmic ray exposure dating with in situ produced cosmogenic 3He: results from young Hawaiian lava flows. Earth and Planetary Science Letters 97, 177–189.

Kurz, M.D., 1986a. Cosmogenic helium in a terrestrial Igneous rock. Nature 320, 435–439.

Kurz, M.D., 1986b. In situ production of terrestrial cosmogenic helium and some applications to geochronology. Geochimica et Cosmochimica Acta 50, 2855–2862.

Kurz, M.D., 1987. Erratum. Geochimica et Cosmochimica Acta 51, 1019.

Lal, D., 1987. Production of He-3 in terrestrial rocks. Chemical Geology.

Lal, D., 1991. Cosmic ray labeling of erosion surfaces: *in situ* nuclide production rates and erosion models. Earth and Planetary Science Letters 104, 424–439.

Licciardi, J.M., Kurz, M.D., Clark, P.U., Brook, E.J., 1999. Calibration of cosmogenic ^{3}He production rates from Holocene lava flows in Oregon, USA, and effects of the Earth's magnetic field. Earth and Planetary Science Letters 172, 261–271.

Licciardi, J.M., Clark, P.U., Brook, E.J., Pierce, K.L., Kurz, M.D., Elmore, D., Sharma, P., 2001. Cosmogenic ^{3}He and ^{10}Be chronologies of the late Pinedale northern Yellowstone ice cap, Montana, USA. Geology 29, 1095–1098.

Licciardi, J.M., Clark, P.U., Brook, E.J., Elmore, D., Sharma, P., 2004. Variable response of western U.S. glaciers during the last deglaciation. Geology 32, 81–84.

Licciardi, J., Kurz, M., Curtice, J., 2006. Cosmogenic ^{3}He production rates from Holocene lava flows in Iceland. Earth and Planetary Science Letters 246, 251–264.

Lifton, N.A., Jull, A.J.T., Quade, J., 2001. A new extraction technique and production rate estimate for in situ cosmogenic ^{14}C in quartz. Geochimica et Cosmochimica Acta 65, 1953–1969.

Lifton, N.A., Bieber, J.W., Clem, J.M., Duldig, M.L., Evenson, P., Humble, J.E., Pyle, R., 2005. Addressing solar modulation and long-term uncertainties in scaling secondary cosmic rays for in situ cosmogenic nuclide applications. Earth and Planetary Science Letters 239, 140–161.

Masarik, J., Beer, J., 1999. Simulation of particle fluxes and cosmogenic nuclide production in the Earth's atmosphere. Journal of Geophysical Research 104, 12099–12111.

Masarik, J., Reedy, R.C., 1995. Terrestrial cosmogenic-nuclide production systematics calculated from numerical simulations. Earth and Planetary Science Letters 136, 381–395.

Masarik, J., 2002. Numerical simulation of in-situ production of cosmogenic nuclides. Geochimica et Cosmochimica Acta 66, A491.

Oviatt, C.G., Nash, W.P., 1989. Late Pleistocene basaltic ash and volcanic-eruptions in the Bonneville Basin, Utah. Geological Society of America Bulletin 101, 292–303.

Oviatt, C.G., Currey, D.R., Sack, D., 1992. Radiocarbon chronology of Lake Bonneville, Eastern Great Basin, USA. Palaeogeography Palaeoclimatology Palaeoecology 99, 225–241.

Poreda, R.J., Cerling, T.E., 1992. Cosmogenic Neon in recent lavas from the western United States. Geophysical Research Letters 19, 1863–1866.

Putnam, A., Schaefer, J.M., Vandergoes, M., Barrell, D., Denton, G.H., Kaplan, M., Schwartz, R., Finkel, R.C., Goehring, B.M., Kelley, S.E., 2010. In situ cosmogenic 10Be production rate from the Southern Alps, New Zealand. Quaternary Geochronology 5 (4), 392–409.

Reimer, P.J., Baillie, M.G.L., Bard, E., Bayliss, E., Beck, J.W., Bertrand, C., Blackwell, P.G., Buck, C.E., Burr, G., Cutler, K.B., Damon, P.E., Edwards, R.L., Fairbanks, R.G., Friedrich, M., Guilderson, T.P., Hughen, K.A., Kromer, B., McCormac, F.G., Manning, S., Bronk Ramsey, C., Reimer, R.W., Remmele, S., Southon, J.R., Stuiver, M., Talamo, S., Taylor, F.W., van der Plicht, J., Weyhenmeyer, C.E., 2004. INTCAL04 terrestrial radiocarbon age calibration, 0–26 cal kyr BP. Radiocarbon 46, 1029–1058.

Sack, D., 1999. The Composite nature of the Provo level of Lake Bonneville, Great Basin, Western North America. Quaternary Research 52, 316–327.

Schäfer, J.M., Ivy-Ochs, S., Wieler, R., Leya, I., Baur, H., Denton, G.H., Schlüchter, C., 1999. Cosmogenic noble gas studies in the oldest landscape on earth: surface exposure ages of the Dry Valleys, Antarctica. Earth and Planetary Science Letters 167, 215–226.

Schäfer, J.M., Baur, H., Denton, G.H., Ivy-Ochs, S., Marchant, D.R., Schlüchter, C., Wieler, R., 2000. The oldest ice on Earth in Beacon Valley, Antarctica: new evidence from surface exposure dating. Earth and Planetary Science Letters 179, 91–99.

Stone, J.O., 2000. Air pressure and cosmogenic isotope production. Journal of Geophysical Research 105, 23753–23759.

Trull, T.W., Kurz, M.D., Jenkins, W.J., 1991. Diffusion of cosmogenic He-3 in olivine and quartz-implications for surface exposure dating. Earth and Planetary Science Letters 103, 241–256.